CONSTRAINING THE ROTATION RATE OF TRANSITING EXTRASOLAR PLANETS BY OBLATENESS MEASUREMENTS

S. Seager[a] and Lam Hui[b]

[a]Institute for Advanced Study, Einstein Drive, Princeton, NJ 08540; seager@ias.edu
[b]Department of Physics, Columbia University, 538 West 120th Street, New York, NY 10027; lhui@astro.columbia.edu

Draft version 2008 February 1

ABSTRACT

The solar system gas giant planets are oblate due to their rapid rotation. A measurement of the planet's projected oblateness would constrain the planet's rotational period. Planets that are synchronously rotating with their orbital revolution will be rotating too slowly to be significantly oblate; these include planets with orbital semi-major axes $\lesssim$ 0.2 AU (for $M_P \sim M_J$ and $M_* \sim M_\odot$). Jupiter-like planets in the range of orbital semi-major axis 0.1 AU to 0.2 AU will tidally evolve to synchronous rotation on a timescale similar to main sequence stars' lifetimes. In this case an oblateness detection will help constrain the planet's tidal Q value.

The projected oblateness of a transiting extrasolar giant planet is measurable from a very high-photometric-precision transit light curve. For a sun-sized star and a Jupiter-sized planet the normalized flux difference in the transit ingress/egress light curve between a spherical and an oblate planet is a few to 15×10^{-5} for oblateness similar to Jupiter and Saturn respectively. The transit ingress and egress are asymmetric for an oblate planet with an orbital inclination different from 90° and a non-zero projected obliquity. A photometric precision of 10^{-4} has been reached by HST observations of the known transiting extrasolar planet HD 209458 b. Kepler, a NASA discovery-class mission designed to detect transiting Earth-sized planets requires a photometric precision of 10^{-5} and expects to find 30 to 40 transiting giant planets with orbital semi-major axes < 1 AU, about 20 of which will be at > 0.2 AU. Furthermore, part-per-million photometric precision (reached after averaging over several orbital periods) is expected from three other space telescopes to be launched within the next three years. Thus an oblateness measurement of a transiting giant planet is realistic in the near future.

Subject headings: planetary systems — planets and satellites: general

1. INTRODUCTION

Extrasolar transiting planets are suitable for a variety of followup measurements while they transit their parent star. Many of the followup measurements would aim to detect additional planet components that block light from the parent star, such as moons, rings, or the planet's atmosphere. Recently, the atmosphere of the transiting planet HD 209458 b was detected in transmission in the neutral sodium resonance line (Charbonneau et al. 2002). A followup measurement of a transiting planet's albedo and phase curve would also be very useful in constraining atmosphere properties since both the radius and orbital inclination (i) are known (Seager, Whitney, & Sasselov 2000). Here we describe an additional planet property that can be derived from followup measurements of transiting extrasolar planets: the planet's projected oblateness. The oblateness is defined as $(R_e - R_p)/R_p$ where R_e is the planet's equatorial radius and R_p the planet's polar radius. The solar system gas giants all have a significant oblateness, ranging from 0.02 to 0.1, due to their rapid rotation. Saturn's oblateness is so large it is obvious from whole-planet images. An oblateness detection would immediately tell us that a planet is a rapid rotator.

A planet's oblateness signature on a transit light curve was first described in Hui & Seager (2002). The oblateness signature is expected to be small. However, recent obser-vations by HST/STIS (Brown et al. 2001) reached an unprecedented photometric precision of 10^{-4}, and space telescopes MOST (Canadian Space Agency; launch date December 2002), MONS (Danish Space Agency; launch date $\sim$ 2004), Corot (French Space Agency, European Space Agency, launch date 2004), and Kepler (NASA; launch date 2006) are designed to reach photometric precision of a few$\times 10^{-6}$ by averaging measurements over several orbital periods. Kepler, a wide-field transit search with the main goal of detecting Earth-sized planets orbiting solar type stars, expects to find 30–40 transiting extrasolar giant planets. With the prospect of high photometric precision, we investigate the transit signature of an oblate giant planet and the constraints on an oblate extrasolar planet's rotational period and tidal Q value.

2. OBLATENESS AND ROTATIONAL PERIOD

Here we review the relation between oblateness and rotational period (see e.g. Collins 1963; van Belle et al. 2001), making the simplest assumptions about the structure of the planets in question. The potential for a uniformly rotating body has two terms, gravitational and rotational. The gravitational potential for a rotating, not too aspherical, figure of equilibrium can be expanded using the Legendre polynomials (see e.g. Danby 1962; Chan-

drasekhar 1969),

$$\phi_g = -\frac{GM_P}{R}\left(1 - \frac{J_2}{R^2}\frac{1}{2}(3\cos^2\theta - 1) - \ldots\right), \qquad (1)$$

where G is the Universal gravitational constant, M_P is the planet mass, R is the planet surface radius, J_2 is a constant coefficient, and θ is the angle measured from the planet's rotation axis. The gravitational moments, of which J_2 is an example, describe the structure and shape of a rotating fluid and are measured for the solar system planets by precession rates of satellite and ring orbits and by spacecraft trajectories. The gravitational moments are not known for extrasolar planets, but they generally contribute small corrections to the gravitational potential. Here, we keep only the first term of equation (1), the gravitational potential of a point mass.

The rotational potential ϕ_r arises from the force of centripetal acceleration. For a rigid body[1] rotating at angular velocity w about the z axis,

$$\phi_r = -\frac{1}{2}w^2(x^2 + y^2) = -\frac{1}{2}w^2 R(\theta)^2\sin^2\theta, \qquad (2)$$

where the right hand side term is in spherical polar coordinates, and for axisymmetric rotation $R = R(\theta)$. Hence the total potential $\phi = \phi_g(\theta) + \phi_r(\theta)$ for a rigid rotator with a gravitational point mass potential is

$$\phi = -\frac{GM_P}{R(\theta)} - \frac{1}{2}w^2 R(\theta)^2\sin^2\theta. \qquad (3)$$

We can use the fact that the total potential ϕ is constant on the surface (Eddington 1926) to consider that ϕ at the pole ($\theta = 0$) and at the equator ($\theta = \pi/2$) are the same. Then equation (3) can be written as,

$$\frac{GM_P}{R_p} = \frac{GM_P}{R_e} + \frac{1}{2}w^2 R_e^2, \qquad (4)$$

where the polar radius R_p corresponds to the rotation axis z, and R_e is the equatorial radius.

Then considering the definition of oblateness, $\eta \equiv (R_e - R_p)/R_p$,

$$\omega^2 = \frac{2GM_P}{R_e^3}\eta, \qquad (5)$$

and the rotational period $P = 2\pi/\omega$ is

$$P = 2\pi\sqrt{\frac{R_e^3}{2GM_P}\frac{1}{\eta}}. \qquad (6)$$

Note that with e as the eccentricity (hereafter called ellipticity to avoid confusion with eccentricity of the planet's orbit) of an ellipse, $R_p = R_e\sqrt{1 - e^2}$, and so

$$\eta \equiv \frac{(R_e - R_p)}{R_p} = \frac{1}{\sqrt{1 - e^2}} - 1. \qquad (7)$$

The maximum oblateness can be estimated by considering the centripetal acceleration for a given planet mass and radius that can prevent the body from flying apart,

(again, ignoring higher order terms in the gravitational potential). Considering a particle at $r = R_e$ and $\theta = \pi/2$, $GM_P m/R_e^2 = m\omega^2 R_e$, and considering the relation between the angular velocity ω and the oblateness η (equation (5)), the maximum possible oblateness is $\eta = 0.5$, which corresponds to an ellipticity of $e = 0.745$.

It is clear, considering equation (6), that a measurement of the oblateness η, together with the measurement of M_P and R_P (here defined as $R_P = \sqrt{R_e R_p}$) from the transit photometry and radial velocity data, will yield the planet's rotational period, subject to two considerations. The first is that the ϕ_g is expected to deviate from a point mass potential, since the solar system gas giant planets have non-zero J_2 and higher order moments. Secondly only the projected oblateness can be measured and hence only an upper limit on the rotational period can be obtained. To be precise, suppose the three-dimensional ellipticity is e, the projected ellipticity equals $e(1 - \cos^2\alpha)$ where α is the angle between the axis of planet rotation and the line of sight to the planet (see Appendix A of Hui & Seager 2002). To the extent the angle α is random, one expects on average that the projected ellipticity is half the actual value. The projected oblateness can be obtained from the projected ellipticity using the relation between η and e in equation (7). *Hereafter, whenever we refer to ellipticity e or oblateness η, we mean its projected version, unless otherwise stated.*

3. TIMESCALE FOR TIDAL SYNCHRONIZATION OF ROTATION

Planetary oblateness is caused by rapid rotation. Planets that rotate synchronously with their orbital period will generally be rotating too slowly to be significantly oblate. Therefore, the tidal evolution timescale for synchronous rotation will limit the parameter space—mainly the orbital semi-major axis D—where oblate planets are expected to be found. Conversely, a detection of oblateness for a planet together with an estimation of the system's age could help to constrain the planet's tidal dissipation factor Q (we will refer to it as Q_P here). The synchronous rotation timescale is (e.g. Goldreich & Soter 1966; Zahn 1977; Hubbard 1984; Guillot et al. 1996)

$$t_{sync} \approx Q_P\left(\frac{R_P^3}{GM_P}\right)\omega\left(\frac{M_P}{M_*}\right)^2\left(\frac{D}{R_P}\right)^6, \qquad (8)$$

where $\omega = |\omega_I - \omega_{orb}| \simeq \omega_I$, where ω_I is the planet's primordial rotational angular velocity and ω_{orb} its orbital angular velocity, R_* and M_* are the star's radius and mass, and G is the universal gravitational constant. Q_P is inversely related to the tidal dissipation energy. For a Jupiter-like planet (with Jupiter's tidal $Q_P = 10^5$ (Ioannou & Lindzen 1993) and Jupiter's current rotation rate $\omega_I = \omega_{Jupiter} = 2\pi/9.92$h) orbiting at 0.05 AU around a solar twin, $t_{sync} = 2 \times 10^6$ years. For HD 209458 b, with $R_* = 1.18 M_\odot$, $M_* = 1.06 M_\odot$, $R_P = 1.42 R_J$, (Cody & Sasselov 2001; Brown et al. 2001), $M_P = 0.69 M_J$ (Mazeh et al. 2000), $t_{sync} = 4 \times Q_P$ years. Because HD 209458 b has $t_{sync} \ll t_*$ (where t_* is the age of the parent star), synchronous rotation is expected to have been reached.

---

[1]The gas giant planets have differential rotation. The slight deviation from rigid body rotation is due to convective redistribution of angular momentum.

Note that planets of Jupiter's mass, Q_P, and ω_I orbiting a sun-mass star with $D \lesssim 0.2$ AU will be synchronous rotators.

The tidal synchronization timescale has as its main uncertainty Q_P and ω_I. It is interesting to compare t_{sync} with the typical ages of stars (t_*) with known extrasolar planets: one to a few billion years. Figure 2a shows t_{sync} as a function of D and $Q_P M_P / M_*^2$ to illustrate that planets with $D \sim 0.15$ to 0.4 AU have t_{sync} similar to these typical ages of stars with known planets. Of the parameters in equation (8), D, M_P, R_P can be measured for a transiting planet and M_* can be well estimated. Therefore Q_P can be constrained with: an oblateness measurement as evidence for non-synchronous rotation; an assumption for ω_I; a planet with D such that $t_{sync} \sim t_*$. (Note that Q_P can also be constrained by considering the tidal evolution time for tidal circularization, but in this case the values for M_P and R_P in specific cases are not known.)

In addition to the planet's rotation rate, other orbital parameters will evolve as a consequence of tides raised on the planet by the star. The orbital circularization timescale (Goldreich & Soter 1966) and the timescale for co-planarity (defined as the coincidence of the planet orbital plane and the stellar equatorial plane) are both longer than the synchronous rotation timescale (Rasio et al. 1966; Hut 1981). The planet's projected obliquity, β (defined here as the *projected* angle of inclination of the planet's rotation axis to the planet's orbit normal) is measurable for a transiting oblate planet (see §4) that has an orbital inclination different from $90°$. The planet's obliquity is also affected by tidal evolution. The timescale for tidal evolution to zero obliquity is the same as the tidal synchronous rotation timescale for a planet in a circular orbit (Peale 1999). For eccentric orbits the obliquity evolution is complex and coupled to other orbital evolution timescales (Peale 1999). However, a detection of obliquity together with other measured orbital and physical parameters for a planet in the tidal evolution regime will be useful to constrain the planet's evolutionary history. Note that a planet may escape evolving to synchronous rotation (or to a circular orbit and zero obliquity) in the presence of other nearby planets. HD 83443 (Mayor et al. 2002) is an interesting example described in Wu & Goldreich (2002).

4. RESULTS AND DISCUSSION

4.1. *Transit Computation*

We want to determine the shape and magnitude of the transit light curve due to an oblate planet with different values of projected obliquity. Because the effect is small compared to a spherical planet transit, the transit light curve must be computed to high accuracy, $\lesssim 10^{-7}$, in order to accurately calculate effects at the $\sim 10^{-5}$ level. We use planetocentric coordinates and consider the projected oblate planet to be an ellipse. The planet's surface is described by the ellipse equation in polar coordinates,

$$r^2 = R_e^2 \frac{1 - e^2}{(1 - e^2 \cos^2(\Theta + \beta - \pi/2))}, \qquad (9)$$

where r is the distance from planet center and Θ is measured from the projected orbit normal. In this coordinate

system, the star's surface is represented by

$$R_*^2 = (r\cos\Theta \pm D\cos i \cos\omega_{orb}(t-t_0))^2 + (r\sin\Theta + D\sin\omega_{orb}(t-t_0))^2 \qquad (10)$$

where ω_{orb} is the orbital angular velocity, t is time, and t_0 is the time of transit center. We consider the intersection of the equations for the planet and star in order to determine (1) start and end of ingress and egress and (2) integration limits for the star area blocked by the planet.

4.2. *The Shape and Amplitude of the Oblateness Signature*

The oblateness signature on a transit light curve will be small. In order to quantify the shape and magnitude of the oblate planet's transit signature we compare an oblate planet transit light curve ($T_{ellipse}$) to a spherical planet transit light curve (T_{sphere}) for planets of the same projected area transiting the same sized star. We define $F = [T_{sphere}(t) - T_{ellipse}(t)]$ where F is the flux difference[2] between a spherical planet (projected to a disk) and an oblate planet (projected to an ellipse) transit light curve. The ellipse and projected sphere are always chosen to have the same total area i.e. the minimum of T_{sphere} and the minimum of $T_{ellipse}$ are the same in the absence of limb darkening. Each transit light curve is normalized to the stellar flux. Figure 2b shows the maximum value of F for different e and R_P/R_*. The parameters $i = 90°$ and $\beta = 0°$ are chosen for this figure—as we will see, this gives the weakest oblateness signature, and so the contours in Figure 2b give conservative estimates of the required photometric precision to detect oblateness.

The transit light curve of a Jupiter-sized planet transiting a sun-sized star with orbital inclination $i = 90°$ is shown in Figure 3a. The round-bottomed transit is due to limb darkening, in this case the solar limb-darkening value at 450 nm is used (Cox 2000). At this blue wavelength the sun is strongly limb darkened. The flat-bottomed transit was computed neglecting limb darkening, or in a very non-limb-darkened color (e.g. at IR wavelengths, although solar limb darkening is minor at I band) chosen to illustrate the range of possibilities. On the scale in Figure 3a, transits due to oblate and spherical planets are difficult to tell apart; we show their difference in subsequent panels. In Figure 3 and in this subsection we consider planets with the same area as Jupiter. Because Jupiter is oblate (with $R_e = 7.1492 \times 10^7$m and $R_p = 6.7137 \times 10^7$m), Jupiter's area corresponds to a sphere with effective radius 6.9280×10^7m. Figure 3b shows the flux difference $F = [T_{sphere}(t) - T_{ellipse}(t)]$ between the non-limb-darkened transit light curve of a spherical planet and an oblate planet with ellipticity e varying from 0.1 to 0.4. These transit light curves were computed for an orbital distance $D = 0.2$, but for the case of $i = 90°$ the transit time scales as $D^{1/2}$. The flux difference F in Figure 3b is as high as 1.5×10^{-4} for an planet with ellipticity $e = 0.4$, corresponding to the oblateness of Saturn.

The oblate planet transit signature can be explained as follows. At the start of ingress, when just a small fraction of the planet has crossed the stellar limb, an oblate planet (projected to an ellipse) covers less area on the stellar disk than a sphere (projected to a disk). Hence F (which is actually the flux difference of the light deficit of a disk and

---

[2]Note that this definition of F is different from that in Hui & Seager (2002).

ellipse) is higher. As ingress progresses, the area of the star blocked by an oblate planet decreases compared to the sphere, until the ingress midpoint. At the midpoint of ingress, when the planet center coincides with the stellar limb, the area of the stellar disk that is blocked is roughly the same for an ellipse and a sphere (except for the deviation of the star limb from a straight line); hence the fractional difference at mid-ingress is close to zero. ($F \simeq 0$ at mid-ingress or mid-egress only for $i = 90°$ and $R_P \ll R_*$). The difference F also eventually reaches around 0 towards the middle of the transit between ingress and egress. Another way to consider the oblate transit signature is that for an oblate planet (with larger R_e than a spherical one of the same area), the "first contact" will occur earlier, and the "second contact" will occur later, thus explaining the sign of the difference signal F.

Figure 3c shows the same flux differences (Fs) as in Figure 3b, but at the highly-limb-darkened color of 450 nm. In the presence of strong limb darkening, the maximum value of the oblateness signature at ingress/egress is lower than in the case of no limb darkening (Figure 3b). This is because ingress and egress occur at the stellar limb where a given area takes out less luminosity than from closer to star center. Because of limb darkening the planet transit light curve is asymmetric around mid-ingress. While this is also true for a spherical planet, the effect is exaggerated for an ellipse. Limb darkening also causes a flux difference between an oblate and spherical planet when the planet is fully superimposed on the parent star; however this difference is negligible compared to the oblateness signature at ingress and egress.

In all of the above cases, Figure 3a-c, $i = 90°$ and $\beta = 0$ is assumed. An oblate planet with $i < 90°$ and non-zero projected obliquity β has an interesting transit light curve. Figure 3d shows the transit light curve for different orbital inclinations (neglecting limb darkening). The dot-dashed line at $i = 88.73°$ shows an almost grazing planet transit. The transit light curves of an oblate planet and of a spherical planet are indistinguishable on the scale of Figure 3d. Figure 3e and Figure 3f show F, the flux difference in the transit light curve between a spherical planet and an oblate planet with $\beta = 45°$ for various orbital inclinations. Note that ingress and egress last longer for transits with larger $\cos i$, making the oblateness signature easier to measure.

The ingress and egress oblateness signatures are completely symmetric about mid-transit (i.e. $F(t) = F(-t)$) for projected obliquity $\beta = 0°$ (cases shown in Figure 3c). The oblateness signature will be more easily measured from a transit light curve that is asymmetric about mid-transit in its ingress and egress. Such an asymmetry will occur in the case of an oblate planet with a non-zero obliquity and with orbital inclination different from 90°. The asymmetry is apparent in comparing Figures 3b and 3e. Figures 4a and b show the asymmetric flux difference $F_{asym} = [T_{ellipse}(t) - T_{ellipse}(-t)]$ for different cases of i and β. The oblate planet considered in Figure 4 has $e = 0.4$ and the same area as Jupiter. Reaching amplitudes of $\sim 2 \times 10^{-4}$ these are close to the current best precision photometry (from HST). The signatures in Figure 4 can be considered maximum signatures using solar system values.

In summary, there are *two* oblateness signatures one can

look for: 1) a detailed difference in light curves between a transit by a sphere and a transit by an ellipse, around ingress and around egress; and 2) an asymmetry of the light curve between ingress and egress in the case of non-zero projected obliquity β and $i \neq 90°$. β and e are not degenerate and can both be extracted from a fit to the light curve. When both signatures can be detected, one can obtain constraints on obliquity as well as oblateness.

We expect to be able to distinguish the oblateness transit signature from other similar magnitude effects during transits. Planetary moons could affect the planet transit light curve but, due to their size, shape, and projected separation from the planet, would not mimic planet oblateness (although they could still cause a transit light curve asymmetry). Planetary rings will be projected into an ellipse unless the inclination of the planet's ring plane to the line of sight is either 0° or 90°. With a few parts-per-million photometric precision, most cases of planetary rings should not be confused with the oblateness signature because the rings have a relatively large radius and a slightly different transit signature than an oblate planet. A planet mass measurement (by radial velocity observations and by the transit to give i) would likely alleviate any confusion due to transiting rings (which would make the planet look much larger) due to the giant planet mass-radius relationship (Guillot et al. 1996). Atmospheric lensing (Hui & Seager 2002) due to a spherical planet may be confused with the oblateness signature. However at wavelengths where the planet's atmosphere is strongly absorbing atmospheric lensing is not present. In addition the transit asymmetry due to a non-zero β is not reproducible by atmospheric lensing. Confusion at the 10^{-5} level from other signals such as star spots, large planetary features, etc. are unlikely and are discussed in Hui & Seager (2002).

4.3. HD 209458 b: The Only Known Transiting Extrasolar Planet

Recently Brown et al. (2001) used HST/STIS to measure the transit light curve of HD 209458 b, the only currently known transiting extrasolar planet (Charbonneau et al. 2000; Henry et al. 2000). The resulting photometric precision is at a level of 10^{-4}. This level of precision is not high enough to measure the expected oblateness of HD 209458 b. The close-in extrasolar giant planets like HD 209458 b are not expected to be significantly oblate due to slow rotational periods resulting from tidal locking to their orbital revolution. Assuming synchronous rotation an orbital period of 3.5 days corresponds to an oblateness of 0.0018 ($e = 0.05$), considering HD 209458 b to be a rigid rotator with $M_P = 0.69 M_J$ (Mazeh et al. 2000) and $R_P = 1.42$ (the most recent derivation from Cody & Sasselov 2001). At an orbital inclination of 86.1° the flux difference from a transit light curve of a sphere has a maximum amplitude of only a few $\times 10^{-6}$. If HD 209458 b has a non-zero projected obliquity (β), the asymmetry of ingress to egress could be as high as 8×10^{-6}. Such an obliquity is not expected, however, due to tidal evolution. Obtaining an upper limit for e and β for HD 209458 b by a fit to a high-precision transit light curve would observationally confirm the expected slow rotational period for HD 209458 b.

4.4. Constraining the EGP Rotation Rate

4

The four solar system gas giant planets have significant oblateness, with values listed in Table 1 (note that oblateness here is the actual oblateness in three dimensions, i.e. not a projected value). With the exception of Jupiter, they all have substantial obliquity with values that are consistent with random β. The solar system gas giant planets have measured rotational periods from 9.92 h to 17.24 h (see Table 1). The rotational periods as calculated from equation (6) using the measured oblateness values are within 20% or less of the actual rotational periods. The estimated rotational periods are consistently low, due to the neglect of the higher order gravitational moments in the gravitational potential (equation (1)).

For extrasolar planet transit measurements only the projected oblateness can be measured, and hence only an upper limit on the rotational period can be obtained. With a measurement of the rotation rate together with the projected oblateness β could be constrained. The rotational period could be directly measurable with the next generation of radio telescopes for Jupiter-like planets with high synchrotron emission (like Jupiter) (Bastian, Dulk, & Leblanc 2000). Note that spectral line measurements may give information on winds in the planet atmosphere rather than the planet's rotation rate.

5. SUMMARY

An oblate planet and a spherical planet of Jupiter's area orbiting a sun-like star will have different ingress and egress transit light curves by as much as a few to 15 $\times 10^{-5}$. A planet's oblateness is most easily detectable in the case where the planet's orbital inclination is different from edge-on, and the planet's projected obliquity is substantially different from zero. In this case the transit light curve is asymmetric between the ingress and egress (see Figure 1 and Figure 4), a signature that can be detected by folding the light curve around mid-transit. The oblateness signature due to a planet with zero projected obliquity is symmetric in ingress and egress; the oblateness can then be measured using a model fit to the data (by exploiting the detailed differences in the light curves produced by a sphere and an ellipse; see Figure 2). The Kepler mission is expected to find 30 to 40 transiting giant planets with orbital semi-major axes < 1 AU, about 20 of which will be at $D > 0.2$ AU, and Kepler and three other space telescopes will reach part-per-million photometric precision. The future is promising for the oblateness measurement of extrasolar planets.

REFERENCES

Bastian, T. S., Dulk, G. A., & Leblanc, Y. 2000, ApJ, 545, 1058

Brown, T. M., Charbonneau, D., Gilliland, R. L., Noyes, R. W., Burrows, A. 2001, ApJ, 552, 699

Chandrasekhar, S. 1969, Ellipsoidal Figures of Equilibrium, Yale University Press

Charbonneau, D., Brown, T. M., Latham, D. W., Mayor, M. 2000, ApJ, 529, L45

Charbonneau, D., Brown, T. M., Noyes, R. W., & Gilliland, R. L. 2002, ApJ, 568, 377

Collins, G. W., II. 1963, ApJ, 138, 1134

Cody, A., & Sasselov, D. D. 2001, submitted to ApJ, astro-ph/0111494

Cox, A. N. 2000, Allen's Astrophysical Quantities, (New York: Springer-Verlag)

Danby, J. M. A. 1962, Fundamentals of Celestial Mechanics, (New York: Macmillan)

Eddington, A. 1926, The Internal Constitutions of the Stars, (New York: Dover)

Goldreich, P., & Soter S. 1966, Icarus, 5, 375

Guillot, T., Burrows, A., Hubbard, W. B., Lunine, J. I., & Saumon, D. 1996, ApJL, 459, 35

Hubbard, W. B. 1984, Planetary Interiors, Van Nostrand Reinhold Co., New York

Hui, L., & Seager, S. 2002, ApJ, in press, astro-ph/0103329

Hut, P. 1981, A&A, 99, 126

Ioannou, P. J., & Lindzen, R. S. 1993, ApJ, 406, 266

Mayor, M., Naef, D., Pepe, F., Queloz, D., Santos, N., Udry, S., & Burnet, M. 2002, in Planetary Systems in the Universe: Observation, Formation and Evolution, IAU Symp. 202, Eds. A. Penny, P. Artymowicz, A.-M. Lagrange and S. Russel ASP Conf. Ser., in press

Mazeh, T. et al. 2000, ApJ, 532, L55

Peale, S. J. 1999, ARAA, 37, 533

Rasio, F. A., Tout, C. A., Lubow, S. H., & Livio, M. 1996, ApJ, 470, 1187

Seager, S., Whitney, B. A., & Sasselov 2000, ApJ, 540, 504

van Belle, G. T., Ciardi, D. R., Thompson, R. R., Akeson, R. L., Lada, E. A. 2001, ApJ, 559, 1155

Wu, Y., & Goldreich, P. 2002, ApJ, 564, 1024

Zahn, J. P. 1977, A&A, 57, 383

Planet	Oblateness $\eta \equiv \frac{R_e - R_p}{R_p}$	e	period (h) (measured)	period (h) (calculated)	obliquity
Jupiter	0.0648744	0.34	9.92	8.23	3.12
Saturn	0.0979624	0.41	10.66	9.47	26.73
Uranus	0.0229273	0.21	17.24	13.83	97.86
Neptune	0.0171	0.18	16.11	14.07	29.58

TABLE 1

SOLAR SYSTEM GIANT PLANET OBLATENESS, PERIOD, AND OBLIQUITY FROM COX (2000). ALSO LISTED IS THE PERIOD CALCULATED FROM THE OBLATENESS BY EQUATION (6) (USING M_P AND R_e FROM COX (2000)).
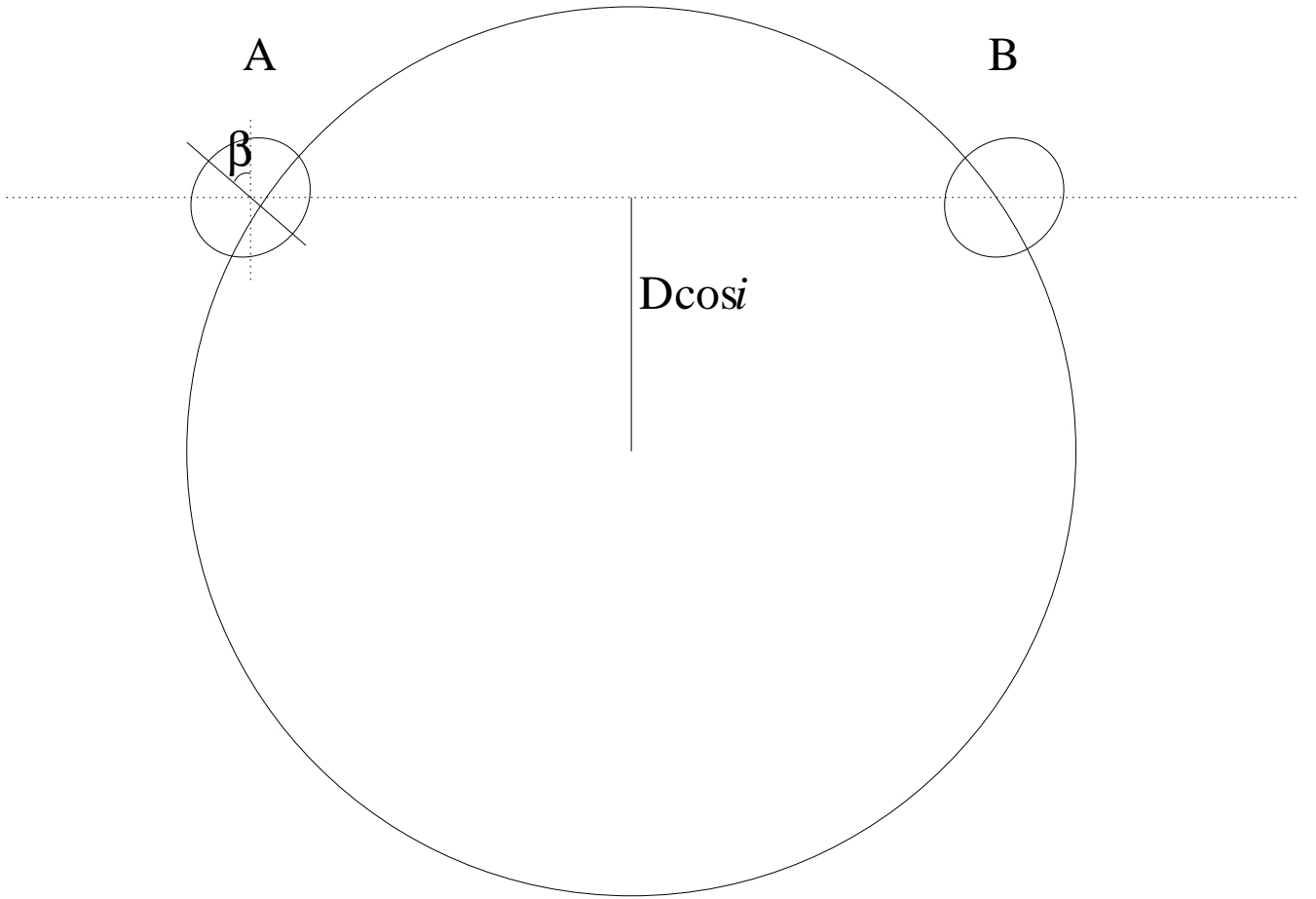
FIG. 1.— Definition of angles. The projected obliquity, β, is the projected angle between the planet's rotation axis and the planet's orbit normal. The orbital inclination is i (where $i = 90°$ corresponds to an edge-on orbit) and D is the semi-major axis. The planet in this schematic diagram has an oblateness equal to that of Saturn (10% which corresponds to $e = 0.4$; note that e in this paper is not orbital eccentricity but is rather related to oblateness, see §2.). For $e > 0$, $i < 90°$, and $\beta > 0°$ the ingress and egress will be asymmetric, for example at points A and B.
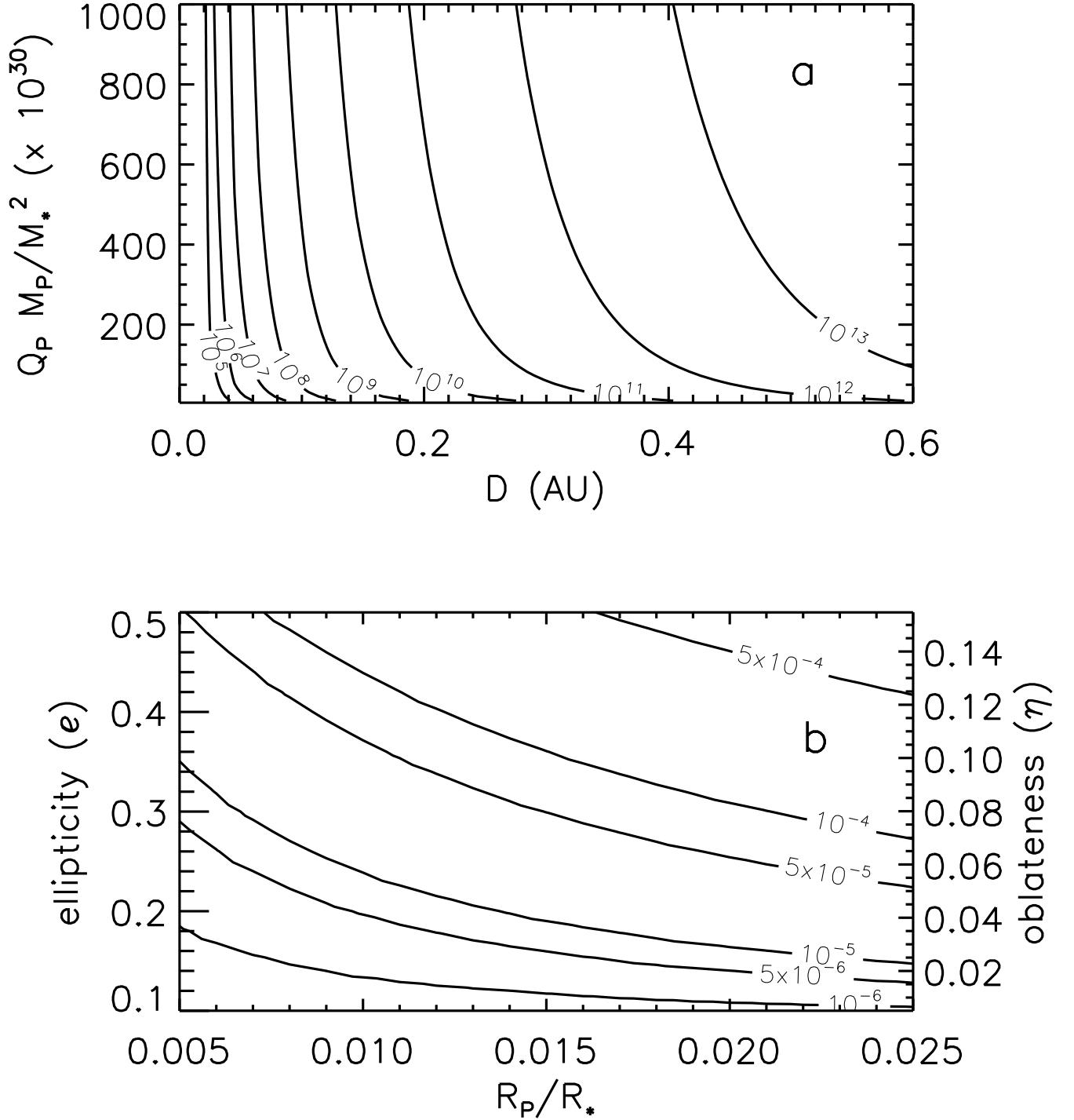
FIG. 2.— Panel a: Synchronization timescales in years (contour lines) for different D, as a function of $Q_P M_P/M_*^2$. Typical ages of stars with known planets are a few billion years; Q_P can be constrained from an oblateness detection with t_{sync} of the same timescale. Note that a serious assumption in computing t_{sync} is that $\omega_I = \omega_{Jupiter} = 2\pi/9.92$ h. Panel b: The photometric precision (contour lines) required to detect a given ellipticity as a function of R_P/R_* (neglecting limb darkening). The parameters $\beta = 0°$ and $i = 90°$ were used; because ellipticity for $\beta > 0°$ and $i < 90°$ is much easier to detect (Figure 4) the required photometric precision can be considered a conservative estimate. The corresponding oblateness, shown on the right y axis, is $\eta = \frac{1}{\sqrt{1-e^2}} - 1$.
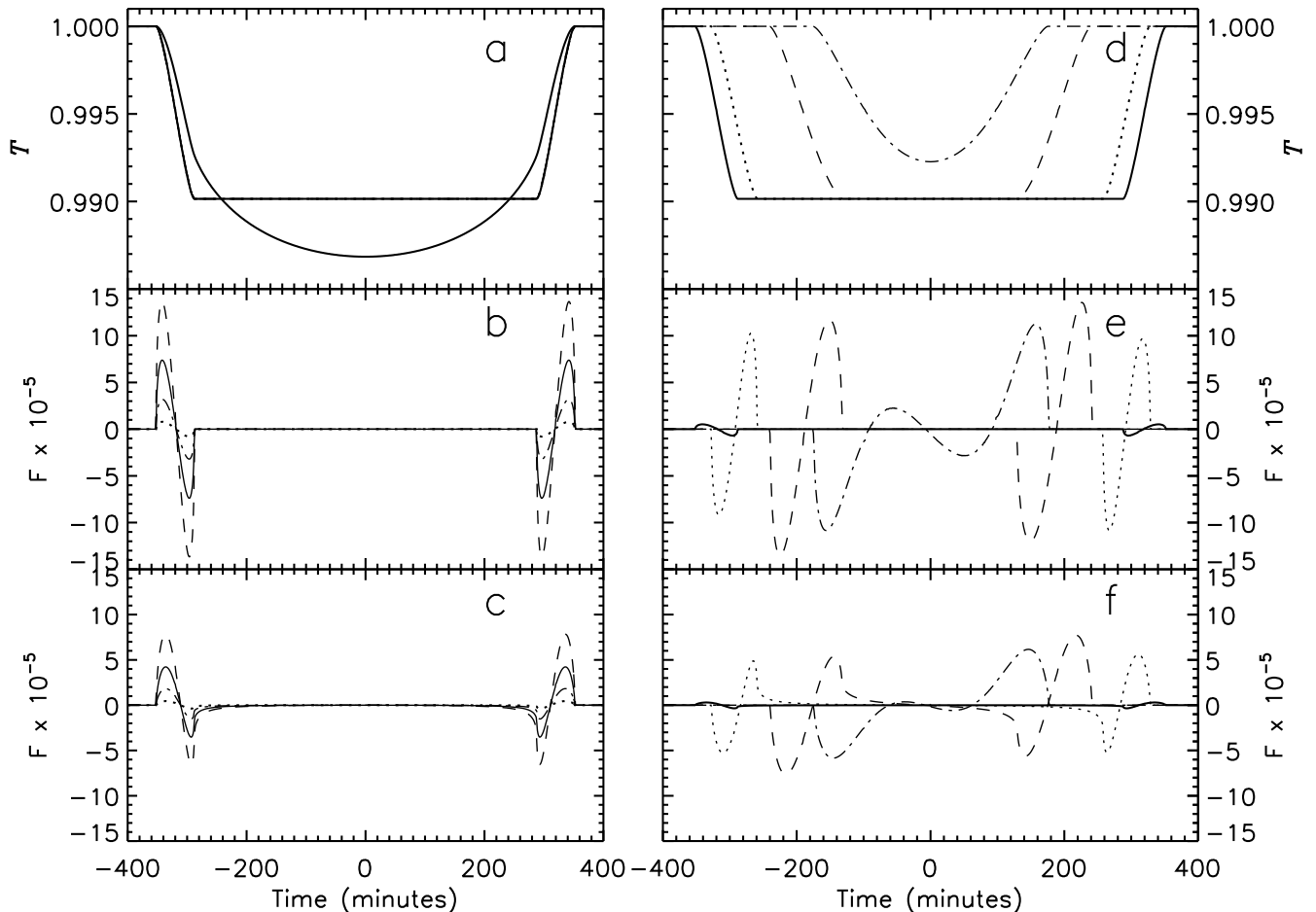
FIG. 3.— A comparison of transit light curves for spherical and oblate Jupiter-sized planets orbiting a sun-sized star. Panel a: The normalized transit light curves (T) at orbital inclination $i = 90°$—on this scale a transit light curve from a spherical planet and an oblate planet are indistinguishable. The round-bottomed curve includes solar limb darkening at 450 nm, whereas the flat-bottomed curved is computed neglecting limb darkening. Panel b: $F = [T_{sphere}(t) - T_{ellipse}(t)]$ (no limb-darkening) where $T_{ellipse}$ is for planets with projected ellipticity $e = 0.1$ (dotted line), $e = 0.2$ (short dashed line), $e = 0.3$ (solid line) and $e = 0.4$ (long-dashed line). Panel c: The same F as in panel b, but at the highly limb-darkened wavelength 450 nm. Panel d: The normalized transit light curve (T) neglecting limb darkening at orbital inclinations $i = 90°$ (solid line), $i = 89.47°$ (dashed line), $i = 88.93°$ (dotted line), and $i = 88.73°$ (dash-dot line). These values of i correspond to impact parameters ($= \cos(i)D/R_*$) 0, 0.4, 0.8, and 0.95 respectively. Panel e: The flux difference $F = [T_{sphere}(t) - T_{ellipse}(t)]$ at different i (line styles correspond to i in panel d) for a planet with $e = 0.4$ (that of Saturn) and $\beta = 45°$. Panel f: The same F as in panel e, but for solar limb darkening at 450 nm. The transit light curves and F in this figure were computed for $D = 0.2$ AU; for other orbital distances the time axis can be scaled by $(D/0.2\text{AU})^{1/2}$ (exactly for panels a–c and approximately for panels d–f). Note the asymmetry $F(t) \neq F(-t)$ in the transit light curves in panels e–f (see Figure 4).
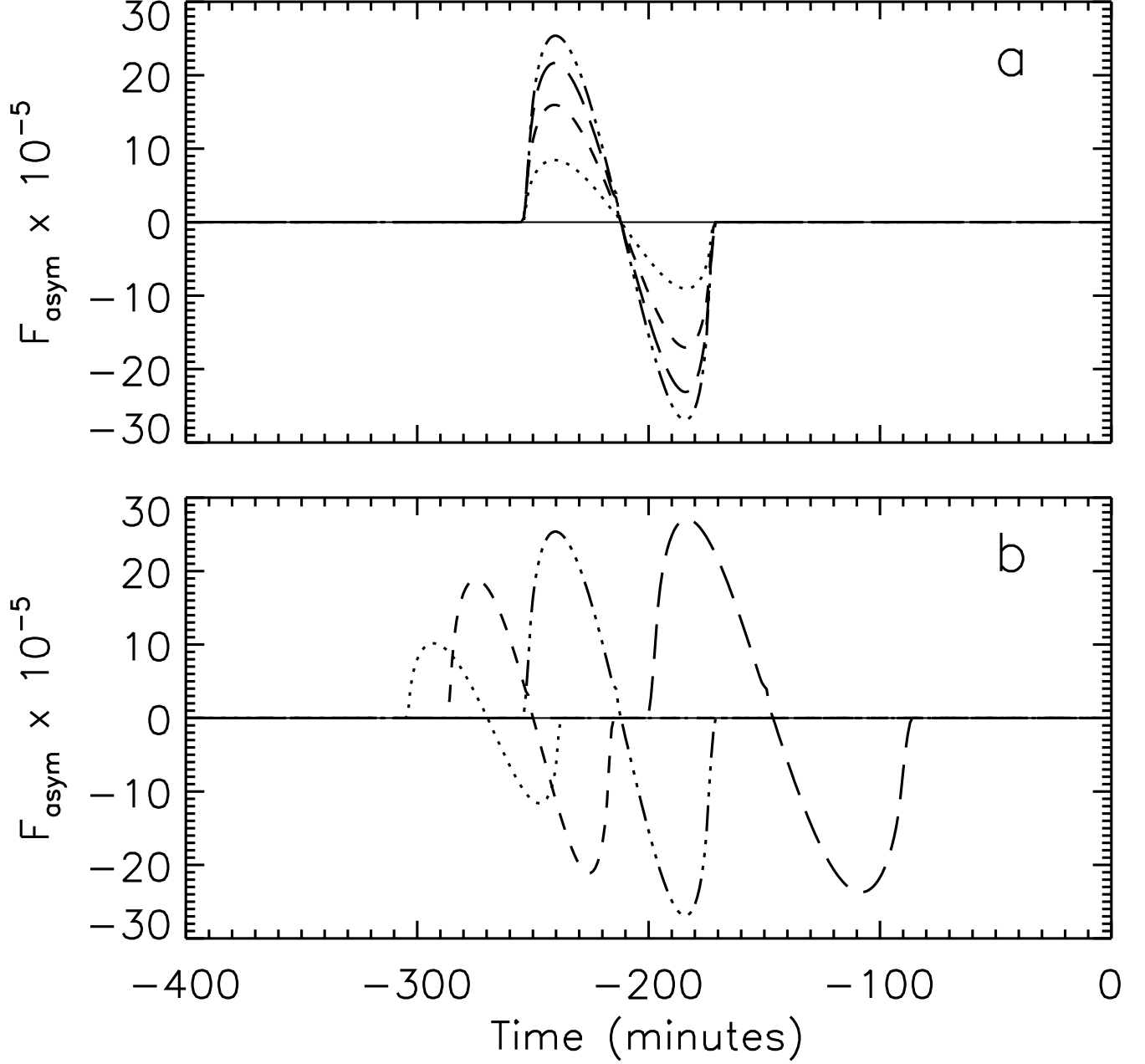
FIG. 4.— The asymmetric flux difference $F_{asym} = [T_{ellipse}(t) - T_{ellipse}(-t)]$ for a Jupiter-sized planet transiting a sun-sized star at $D = 0.2$ AU versus time from mid-transit (neglecting limb darkening). Panel a: F_{asym} for $e = 0.4$ and $i = 89.2°$ (corresponding to an impact parameter of 0.6), with $\beta = 0°$ (solid line), $\beta = 10°$ (dotted line), $\beta = 20°$ (short dashed line), $\beta = 30°$ (long dashed line), and $\beta = 45°$ (dot-dash line). Panel b: F_{asym} for $e = 0.4$ and $\beta = 45°$, with $i = 90°$ (solid line), $i = 89.73°$ (dotted line), $i = 89.47°$ (short dashed line), and $i = 89.20°$ (dot-dash line), and $i = 88.73°$ (long dashed line) The i correspond to impact parameters $(= \cos(i)D/R_*)$ 0, 0.2, 0.4, 0.6, and 0.8, respectively. Note the solid lines in each panel show that there is no transit asymmetry for an oblate planet with $\beta = 0°$ or $i = 90°$.